

**VIKING (VISTA Kilo-degree Infrared Galaxy Survey):**  
**Imaging and Catalogue Data Release 2 (VIKING/batch\_2)**  
**Release date (15th August 2014)**  
**Alastair Edge and Will Sutherland, for the VIKING team**

**Abstract:** The VIKING survey with VISTA (ESO programme ID 179.A-2004) is a wide area (eventually  $\sim 1500$  sq.degrees), intermediate-depth (5-sigma detection limit  $J \sim 21$  on Vega system) near-infrared imaging survey, in the five broadband filters Z, Y, J, H,  $K_s$ .

The planned sky coverage is at high galactic latitudes, and includes two main stripes  $\sim 70 \times 10^\circ$  each: one in the South Galactic cap near Dec  $\sim -30^\circ$ , and one near Dec  $\sim 0^\circ$  in the North galactic cap; in addition, there are two smaller outrigger patches called GAMA09 and CFHLS-W1.

Science goals include  $z > 6.5$  quasars, extreme brown dwarfs, and multiwavelength coverage and identifications for a range of other imaging surveys, notably VST-KiDS and Herschel-ATLAS.

This second public data release of VIKING data covers all of the highest quality data taken between the start of the survey (12th of November 2009) and the end of Period 92 (30th September 2013). This release supercedes the first release (VIKING and VIKING\_CAT published 28.06.2013 and 16.12.2013 respectively) as it includes improved CASU processing (V1.3) that gives better tile grouting and zero point corrections.

This release contains 396 tiles with coverage in all five VIKING filters, 379 of which have a deep co-add in J, and an additional 81 with at least two filters where the second OB has not been executed yet or one filter in an OB was poor quality. These 477 fields cover a total of  $\sim 690$  square degrees and the resulting catalogues include a total of 46,270,162 sources (including low-reliability single-band detections). The imaging and catalogues (both single-band and band-merged) total 839.3GB. The coverage in each of the five sub-areas is not completely contiguous but any inter-tile gaps are relatively small.

### Overview/layout of observations

The basic unit of observations is the VISTA tile, made from combining six offset “pawprints” to fill in gaps between the individual detectors. All VIKING tiles are observed in the default (zero) rotator-sky angle; thus each tile covers a rectangle approximately 1.5 degrees in RA by 1.0 deg in Dec to full exposure.

This data release 2 consists of a total of 477 tiles ( $\sim 690$  sq.deg): this is subdivided into 219 tiles in the Northern Galactic Equatorial Strip (NGP) that covers the GAMA09/12/14 regions, 253 tiles in the Southern Galactic Pole Strip (SGP), and 5 tiles in the CFHLS-W1 region. These comprise most of the data observed up to the end of September 2013, and have overlap with VST-KiDS, the GAMA redshift survey in GAMA09/12/14, the Herschel-ATLAS submm survey (in both GAMA09/12/14 and SGP), and medium-deep CFHT Legacy Survey visible data in W1.

The current coverage is summarised in Figure 1 that plots the distribution of fields in the five filters.

| Region    | RA range           | Dec range          | Tiles |
|-----------|--------------------|--------------------|-------|
| CFHTLS-W1 | 02h 16m to 02h 28m | -6.7 to -2.7 deg   | 5     |
| SGP       | 22h 05m to 03h 32m | -34.0 to -28.0 deg | 253   |
| NGP       | 08h 34m to 14h 58m | -2.0 to +3.0 deg   | 219   |

Table 1: Approximate boundaries of sky coverage for the current release.

### Release content

Exposure times per passband are as given in the following table; note that exposure times per source are the median values (and correspond to pixels with value 100 in the associated confidence-maps); pixels in detector overlap regions receive more exposure, while pixels near the top and bottom in detector x-coordinate (North/South) receive half the median exposure.

| Filter         | Integration/ tile | Integration/ source | Njitter | NDIT x DIT (sec) | Mag.lim (median) |
|----------------|-------------------|---------------------|---------|------------------|------------------|
| Z              | 1440 sec          | 480 sec             | 4       | 1×60s            | 21.4             |
| Y              | 1200 sec          | 400 sec             | 4       | 2×25s            | 20.6             |
| J              | 2×600 sec         | 2×200 sec           | 2×2     | 2×25s            | 20.1             |
| H              | 900 sec           | 300 sec             | 3       | 5×10s            | 19.0             |
| K <sub>s</sub> | 1440 sec          | 480 sec             | 4       | 6×10s            | 18.6             |

Table 2: Integration times per tile, per source (median), number of jitter positions (per pawprint) and individual exposure lengths. Also shows median 10-sigma (Vega) magnitude limit for each passband.

Note that each tile was observed in two separate observing blocks (OBs) of approximately 70 minutes duration each: one for J, Y, Z filters, and the other for J, K<sub>s</sub>, H; these are taken in either order, with the J exposure time divided between the two OBs. The time-span between the two blocks may be months or (sometimes) years; thus, the split J-band is intended to flag objects which may have moved or varied between the two blocks. Observations for band pairs Y/Z and K<sub>s</sub>/H are in one OB, separated by a time-lag typically 25 minutes. The two J-band exposures are coadded to provide a deeper J pawprint. These intermediate pawprints are provided for these deeper co-adds in this release for completeness so accurate variability studies can be performed by comparison with the single epoch tiles in J. In 379 of the 396 cases where two J-band images exist the image quality were well matched so this coaddition was made.

The depth reached is not identical over all fields but none are more than 0.3mag shallower than the medians given in Table 2 as this was our quality threshold for depth. Likewise no field has a seeing worse than 1.2'' as this was the threshold set for image quality.

We have deprecated all fields with an ESO grade of C, R or X that are assigned to incomplete or poor quality OBs by the telescope operator after execution.

The observations in terms of field and filter listed in Table 3 are ones which were released previously but are now deprecated due to falling below the same quality thresholds or having the wrong ESO grade.

## Release Notes

**Previous Releases:** This release is superceeds that made in the first VIKING imaging and catalog (VIKING and VIKING.CAT) releases of October and December 2013 as it uses improved tile grouting and zero point corrections that the latest version of the CASU pipeline (V1.3) provides.

The data reduction follows the standard CASU infrared imaging pipeline from each individual tile image.

In brief, the reduction steps are as follows:

**Reset correction:** This occurs in the data acquisition system, i.e. a VISTA data frame is a difference of two non-destructive detector readouts separated by DIT seconds. Then, NDIT of these frames are co-added within the data acquisition system, before saving to hard disk.

**Dark subtraction:** using exposures with the dark filter inserted, matching the DIT values of the given science exposure.

**Linearity correction:** the VIRCAM detectors show non-linearity, typically a few percent at 10,000 ADUs. A correction polynomial (one per detector) is derived from a fit to observations of the dome screen with varying exposure times, and applied to the counts.

**De-stripping:** this step removes a low-level horizontal striping intrinsic to the VIRCAM detector readout electronics, which is correlated across blocks of 4 detectors.

**Flat-field correction:** the frame is divided by a flat-field frame, derived from a set of twilight sky flats in the matching filter band.

**Bad pixel rejection:** Pixels showing substantial deviance from the linearity frames are masked as bad,

| Field name      | Filters                |
|-----------------|------------------------|
| 00h05-031d26/27 | H, Ks, J_deep          |
| 00h13-032d25    | Y, J_deep              |
| 00h19-032d25    | Y, J_deep              |
| 00h21-033d23    | Z, Y, J_deep           |
| 02h02-031d26/27 | Z, Y, J_deep           |
| 02h09-031d26/27 | Ks, J_deep             |
| 02h09-033d23    | J_deep                 |
| 02h14-030d28/29 | Z, Y, J_deep           |
| 02h19-004d07    | Y, J_deep              |
| 02h19-032d25    | J_deep                 |
| 02h25-003d08    | Z, Y, J_deep           |
| 02h25-005d06/07 | Z, Y, J_deep           |
| 02h26-032d25    | J_deep                 |
| 02h28-031d26/27 | Z, Y, J, H, Ks, J_deep |
| 02h29-033d23    | Z, Y, J_deep           |
| 02h35-033d23    | Z, Y, J_deep           |
| 02h46-032d24/25 | Y, J_deep              |
| 02h47-031d26/27 | H, Ks, J_deep          |
| 08h36+002d25    | Z, Y, J_deep           |
| 08h42-000d28/29 | J_deep                 |
| 08h48+000d28/29 | H                      |
| 08h48+002d25    | Y, J_deep              |
| 09h00+000d28/29 | Y, J_deep              |
| 09h00+001d27    | Ks, J_deep             |
| 09h00-000d28/29 | Y, J_deep              |
| 09h06+000d28/29 | Y, J_deep              |
| 09h06+001d27    | Y, J_deep              |
| 09h11+000d28/29 | Z, Y, J_deep           |
| 09h17+000d28/29 | Ks, J_deep             |
| 09h17+001d26/27 | J_deep                 |
| 09h17+002d25    | Z, Y, J_deep           |
| 09h17-000d28/29 | Ks, J_deep             |
| 11h40-000d28/29 | J_deep                 |
| 11h59+001d26/27 | Z, Y, J_deep           |
| 12h10+001d27    | Y, J_deep              |
| 12h16+001d27    | J_deep                 |
| 14h21+000d28/29 | Y, J_deep              |
| 14h27+000d29    | H, Ks, J_deep          |
| 22h03-032d25    | Z, Y, J, H, Ks, J_deep |
| 22h03-033d23    | Ks, J_deep             |
| 22h10-031d26/27 | Ks, J_deep             |
| 22h10-033d23    | Z, Y, J, H, Ks, J_deep |
| 22h17-031d26/27 | J_deep                 |
| 22h23-031d26/27 | Z, Y, J_deep           |
| 22h24-032d24/25 | Ks, J_deep             |
| 22h37-031d26/27 | Z, Y, J_deep           |
| 22h44-032d25    | J_deep                 |
| 23h19-032d24/25 | Ks, J_deep             |
| 23h26-033d23    | Y, J_deep              |
| 23h39-032d25    | Z, Y, J_deep           |
| 23h46-032d25    | Y, J_deep              |
| 23h58-031d26/27 | Y, J_deep              |
| 23h59-032d25    | Z, Y, J_deep           |

Table 3: Field and filter combinations that were in the First Release but have now failed below the quality and/or ESO grade cuts.

and assigned zero weight in subsequent combinations.

**Sky background correction:** this removes large-scale background variation.

**Jitter stacking:** the set of individual jittered frames for one pawprint-filter combination are combined into a pawprint image, with bad-pixel rejection. These individual pawprint images are available in the data release (see below).

**Photometric and astrometric calibration:** This is based on matching with 2MASS stars (see details below).

**Tiling:** The six individual pawprint images for one filter are combined into a full tile image.

**Grouting:** When combining images into a full tile, there are non-negligible PSF variations, due mainly to seeing variations between the six individual pawprints, and also slight variation in image quality with off-axis distance. Different pairs of pawprints contribute to different regions in the tile, thus the aperture correction varies with position. A specific correction for this (aka “grouting”) is applied to the photometry in the catalogues and is significantly improved in the latest version of the CASU pipeline.

### Astrometric Calibration

The main astrometric calibration is based on 2MASS stars; there are typically 50 unsaturated 2MASS stars per VIRCAM detector, and astrometric transformations from detector coordinates to RA, Dec are derived from these. The typical rms is 0.15 arcsec per star per coordinate, which is dominated by photon noise in the 2MASS data.

External comparisons with UKIDSS and SDSS (in the GAMA09 region) show that the astrometry is good, with typical rms per coordinate around 0.09 arcsec and mean offsets below 0.03 arcsec. Small correlated residuals (generally between pawprints) are seen at the level of approx 0.05 arcsec; these may be improved in a future data release.

### Photometric Calibration

Photometric calibration is also derived from 2MASS stars. A set of colour equations is used to predict VISTA native magnitudes from the observed 2MASS J,H,K<sub>s</sub> colours; these are given by slight modifications of those for UKIDSS (see Hodgkin S. et al., 2009, MNRAS, 394, 675). The adopted VIKING colour terms are:

$$\begin{aligned} Z_V &= J_{2M} + 1.025(J_{2M} - H_{2M}) \\ Y_V &= J_{2M} + 0.610(J_{2M} - H_{2M}) \\ J_V &= J_{2M} - 0.077(J_{2M} - H_{2M}) \\ H_V &= H_{2M} + 0.032(J_{2M} - H_{2M}) \\ K_{sV} &= K_{2M} + 0.01(J_{2M} - K_{2M}) \end{aligned}$$

where in the above, subscript 2M denotes 2MASS and V denotes VIKING. The above equations give the predicted VISTA-system magnitudes of 2MASS stars, and comparing these to instrumental counts for these stars, a zeropoint is determined for each image.

The *internal* photometric zeropoint stability, as deduced from repeated measurements of stars in overlapping regions of adjacent tiles, are stable to  $\sim 0.03$  mag rms.

Externally, comparison against UKIDSS measurements in the GAMA09 region shows good consistency in the H, K<sub>s</sub> bands: the per-tile mean offset is close to zero, and tile-to-tile dispersion in the mean is typically 0.03 mag rms. For bluer bands, there are non-negligible mean zero point offsets, approximately 0.05 mag in J-band and 0.09 mag in the Y-band, both in the sense that VIKING magnitudes are brighter than UKIDSS for the same object. This is probably caused by a combination of two factors: the stellar locus in Y-J, J-K<sub>s</sub> is slightly non-linear, and almost all the matching 2MASS stars are substantially later than A0 spectral type, so the extrapolation of the stellar locus using the above colour terms does not quite pass through (0,0).

The Z band global zeropoint is slightly more uncertain, since the extrapolation from 2MASS is larger, and also the SDSS z-band has a significantly different response function shape (approximately triangular)

from VIKING Z (approximately box-car). Preliminary comparisons suggest the current VIKING Z zeropoint may be too bright by approximately 0.10 mag.

### Star-galaxy classification

A star-galaxy classification parameter (ClassStat) is provided in the list files; this is intended to be approximately Gaussian  $N(0,1)$  for stellar objects, and extends to large positive values for galaxies. Also an integer-based classification (Class); see description below. The band-merged catalogue file (`_finalSourceCat_`) contains also merged statistics based on a quasi-Bayesian combination of the single-band classifications.

In addition to the above, colour-based classification using near-infrared colours (especially including  $K_s$  band) can also provide an effective discriminant between stars and galaxies. For the current dataset, using the Z-J, J- $K_s$  two-colour diagram appears to be the best choice (especially at faint magnitudes where the morphological classification becomes indecisive). This two-colour diagram shows a well-defined boomerang-shaped stellar locus, flattening off near  $J - K_s \sim 0.80$ , and a large cloud of galaxies at redder J- $K_s$  values, typically  $1 < J - K_s < 2$ . (This behaviour is caused by a combination of several factors: late giant stars have redder J- $K_s$  colours than dwarfs; galaxies can have internal extinction, while stars have minimal extinction in these high-latitude fields; and especially the 1.6 micron bump feature in the SED of late-type stars. Redshifting of the 1.6 micron bump towards the  $K_s$  filter causes galaxy J- $K_s$  colours to shift redwards from  $z \sim 0$  to  $z \sim 0.4$ , then flatten off above this).

In future, when visible band (u, g, r, i) data is available from the KIDS survey, even better colour-based classification is likely to be deliverable using for example the (g-i, J- $K_s$ ) two-colour diagram, as shown by Baldry et al (2010, MNRAS 404, 86).

Inspection of samples of “discrepant” objects, defined as those where the morphological and ZJK $_s$  two-colour classifications disagree, shows the following general trends:

- The majority of “discrepant” objects arise from blending issues, e.g. close pairs of objects where the dominant component is a star, or objects affected by halos around bright stars.
- There are a small fraction of genuine blue galaxies close to the stellar colour locus, mostly bright low- $z$  late-type galaxies.
- There are some quasars/AGNs appearing as stellar objects in the red cloud.

### Merging of source catalogues

The released band-merged catalogues are created from the merger of single band catalogues also included in this release. This merging process is outlined in more detail in the VSA documentation but involves the creation of a `vikingSource` table from the individual `vikingDetection` tables. The matching iterates through the catalogues for each band in turn (bluer to redder) and matches can include any combination of filters (one to five) depending on how many filters it is detected in.

These tables are linked via reference ID numbers. The matching is done within a default radius of 2.0 arcsec and the selection between multiple potential matches can be made using the `priOrSec` (primary or secondary) flag. The `PRIMARY_SOURCE` flag has been added to provide an indication which one of the duplicates created in overlap regions between frames should be used. The user is advised to consult with the VSA documentation for more detail about these flags and the merging process.

### Data files and conventions

The imaging data files have the following naming convention:

`viking_er2_HHhMM-DDDdMM_[tile/offN]_F_[type]_NNNNN.ext`

where HHhMM-DDDdMM labels RA/Dec of the pointing centre in hours/minutes of RA, and degrees/arcmins of Dec, `tile/offN` specifies if the image is of a full “tile” or one of the constituent ‘pawprints’ `off0` – `off5`, the filter `F` is one of `z`, `y`, `j`, `h` or `ks`, `type` is whether the file is a FITS image (`image`), confidence map (`conf`) or quicklook jpeg of each of these images (`jpeg`) and the final integer is a unique

identifier assigned by the VSA to each image. Catalogue and jpeg files have numbers NNNNNN matching the parent FITS image, while confidence maps have integer increased by 1 from the matching image. The extension `.ext` denotes file format, and is one of: `.fits.fz` (Rice-compressed FITS file), `.fits` (uncompressed FITS file), or `.jpg` (JPEG image file).

The single band catalogue files in this data release have the following naming conventions:

File names follow the general convention:

`viking_er2_HHhMM-DDDdMM_tile_F_cat_NNNNNNNNNNNN`

Meanings are as follows:

- HHhMM-DDDdMM labels RA/Dec of the pointing centre in hours/minutes of RA, and degrees/arcmins of Dec.
- F gives the filter observed for that observation.
- The twelve-digit integer NNNNNNNNNNNN is a unique identifier assigned by the VSA to each field.

The band-merged catalogue files in this data release have the following naming conventions:

File names follow the general convention:

`viking_er2_HHhMM-DDDdMM_zyjhks_finalSourceCat_NNNNNNNNNNNN`

Meanings are as follows:

- HHhMM-DDDdMM labels RA/Dec of the pointing centre in hours/minutes of RA, and degrees/arcmins of Dec.
- The twelve-digit integer NNNNNNNNNNNN is a unique identifier assigned by the VSA to each field.

### **Entries band-merged catalogues**

The contents of the passband-merged catalogues are given by the **vikingSource** schema of the VSA database ([http://horus.roe.ac.uk/vsa/www/VIKINGDR2/VIKINGDR2\\_TABLE\\_vikingSourceSchema.html](http://horus.roe.ac.uk/vsa/www/VIKINGDR2/VIKINGDR2_TABLE_vikingSourceSchema.html)).

A summary of the most relevant parameters in the band-merged catalogue files is given below:

|  |   |
|--|---|
| <code>ra, dec:</code>  | RA, Dec in J2000 decimal degrees.   |
| <code>l, b:</code>   | Galactic coordinates, decimal degrees.  |
| <code>zXi, zEta, yXi, yEta, etc:</code>  | Source offsets from master position in each of the five bands Z, Y, Y, H, K <sub>s</sub> ; in arcsec East and North respectively.   |
| <code>priOrSec:</code>   | Integer flag for “primary” or “secondary” source. Objects with <code>priOrSec = 0</code> are unique to this tile. Objects with <code>priOrSec = frameSetID</code> are “primary” objects on this tile, with a secondary detection on another tile. Objects with <code>priOrSec&gt;0</code> and <code>priOrSec != frameSetID</code> are “secondary” objects with a “primary” detection on a different tile. |
| <code>zSeqNum, ySeqNum, etc:</code>  | Sequence number, enabling matching this entry to the corresponding single-band detection.   |
| <code>zmyPnt, ymjPnt, jmhPnt, hmksPnt:</code>  | Respectively colours Z-Y, Y-J, J-H, H-K <sub>s</sub> assuming a point source, from the corresponding AperMag3 values.   |
| <code>zmyExt, ymjExt, jmhExt, hmksExt:</code>  | Respectively colours Z-Y, Y-J, J-H, H-K <sub>s</sub> assuming an extended source (using 2 arcsec aperture with no aperture correction).   |
| <code>zAperMag3, zAperMag4, zAperMag6, zAperMagNoAperCorr3, zPetroMag, zSerMag, zPsfMag, etc:</code> | A subset of the various magnitude measures for all the single passbands, beginning with one of z,y,j,h,ks denoting passband. Here, a subset is given to reduce line length: of the many AperMagN values, only AperMag3,4,6 are given here, and the corresponding versions without aperture correction.  |
| <code>zClass, zClassStat, etc:</code>  | Respectively integer and real classification flag for each of the single bands.   |
| <code>mergedClass, mergedClassStat:</code>   | Band-merged integer and real classification, based on a quasi-Bayesian combination of the individual passbands.   |
| <code>pStar, pGalaxy:</code>   | Probability that the object is stellar/galaxy, respectively.  |
| <code>pNoise, pSaturated:</code>   | Probability that the object is noise/saturated, respectively.   |
| <code>zppErrBits, yppErrBits, etc:</code>  | Integer error bits code for each of Z, Y, J, H, K <sub>s</sub> bands. Value Zero = no warnings, 1-255 indicates “Warning” level, and any <code>ppErrBits</code> value >256 indicates potentially more serious problems.   |
| <code>PRIMARY_SOURCE</code>  | Integer flag to select between multiple entries in the catalogue. If the value is 1 then this is the ‘primary’ entry for the source, i.e. <code>priOrSec=0</code> or <code>priOrSec=frameSetID</code> . If the value is 0 then that entry is a duplicated source, usually a source in an overlap region between fields or tiles.  |

We recommend that users should restrict their analysis to objects with `zppErrBits, yppErrBits, etc<255` at all times and `zppErrBits=0` if they require the most reliable subset of the sources. Values of `zppErrBits=16` indicate that the source was deblended, `zppErrBits=64` that at least one bad pixel was within the default aperture and `zppErrBits=128` that the source was low confidence within the default aperture.

### Known problems

As noted in more detail above, there are likely to be modest zero-point offsets ( $\approx 0.06$  mag at J,  $\approx 0.09$  mag at Y-band) in the sense that VIKING magnitudes may be too bright. These appear relatively stable across tiles.

In the current release, the most common source of spurious images is associated with diffraction halos and filter-reflection ghosts around bright stars; these are localised around the parent star, and are easily recognised in the parent images. There are also occasional single-band linear features from artificial satellite trails, meteors or aircraft, which can cause a chain of spurious images. Most such spurious images do not match-up between passbands, therefore multi-band matched detections are generally reliable (especially with 3 or more bands), but we emphasise that **all single-band detections should be treated as unreliable**, unless verified by inspection of images.

There are also “bad patches” on certain detectors, namely a large region on Detector#16 (South-East corner) which does not flat-field well, and a strip along an edge of detector#12 which likewise does not correct well and leads to occasional horizontal lines of spurious images.

Cross-talk between detector channels is essentially negligible.

Image persistence (latent images after a bright star lands on a pixel) is generally small, but not quite

negligible: since VIRCAM has no shutter, very bright stars can occasionally cause curved “streaks” of persistence as they move in non-straight paths during telescope offsets.

There are a small number ( $<100$ ) sources in the single band and band-merged catalogs that have very large ( $>100\text{mag}$ ) errors due to them being close to the detection limit. These sources should be flagged manually and will be excluded in future releases. However, given they are so rare ( $<0.0006\%$  of the band-merged sources) they should not be a major contaminant in any VIKING study.

**Queries** Questions concerning this data release should be addressed initially to [alastair.edge@durham.ac.uk](mailto:alastair.edge@durham.ac.uk).

**Acknowledgements** Please use the following statement in any publication using these data: “This publication has made use of data from the VIKING survey from VISTA at the ESO Paranal Observatory, programme ID 179.A-2004. Data processing has been contributed by the VISTA Data Flow System at CASU, Cambridge and WFAU, Edinburgh”.



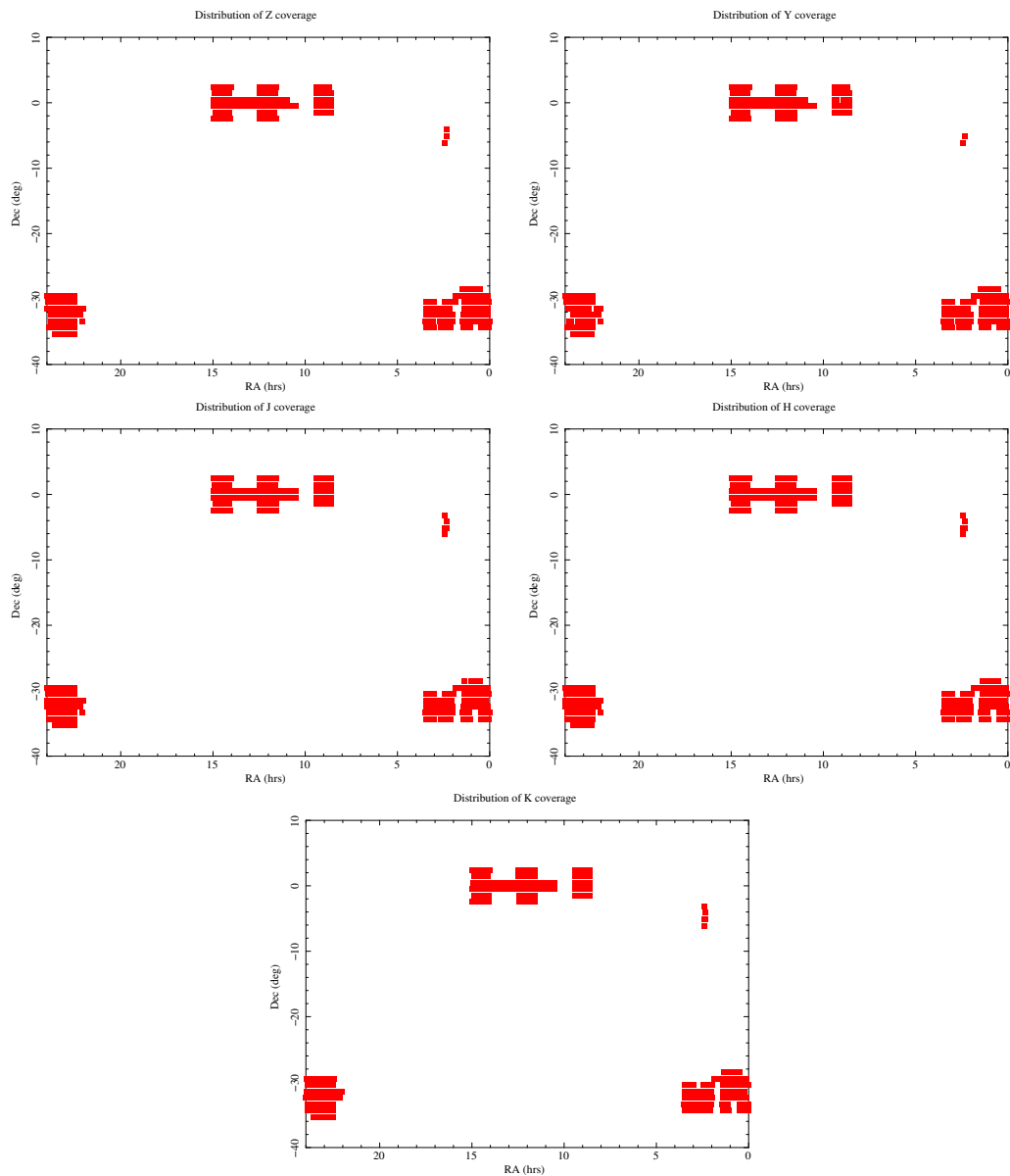


Figure 1: Sky coverage of the fields in this release in terms of filter in order of wavelength (Z, Y, J, H and K).

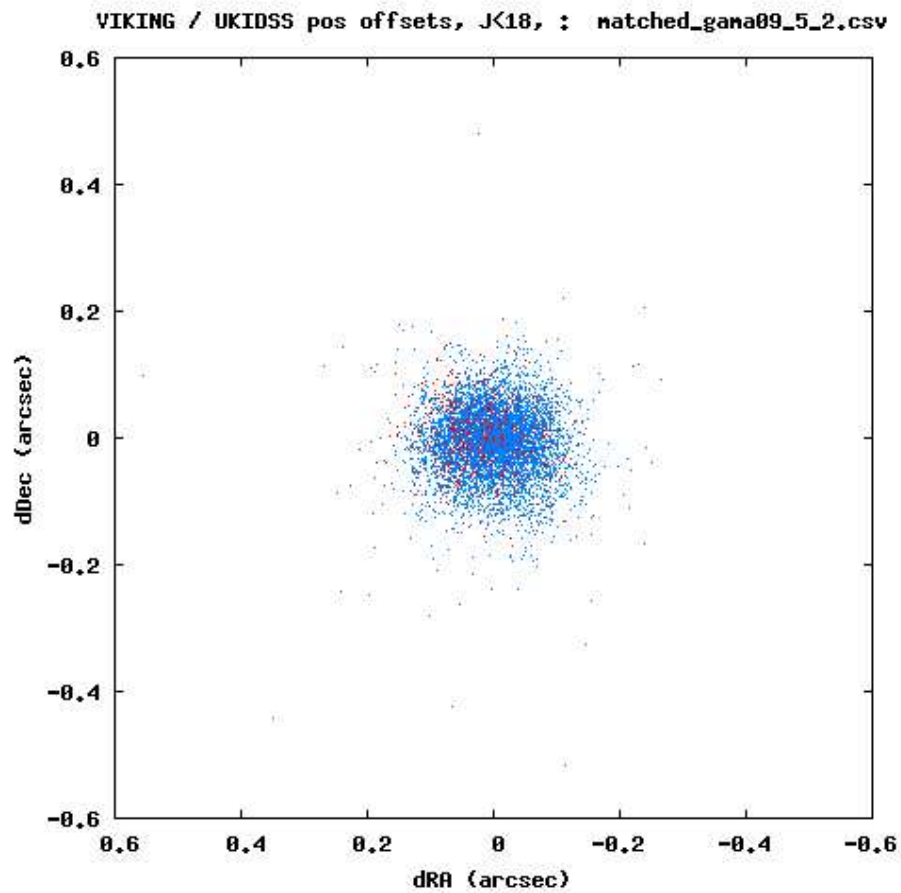


Figure 2: Position offsets in RA, Dec (VIKING-UKIDSS) for one tile, for objects with  $J < 18$ ; stellar objects are blue, extended objects in red.

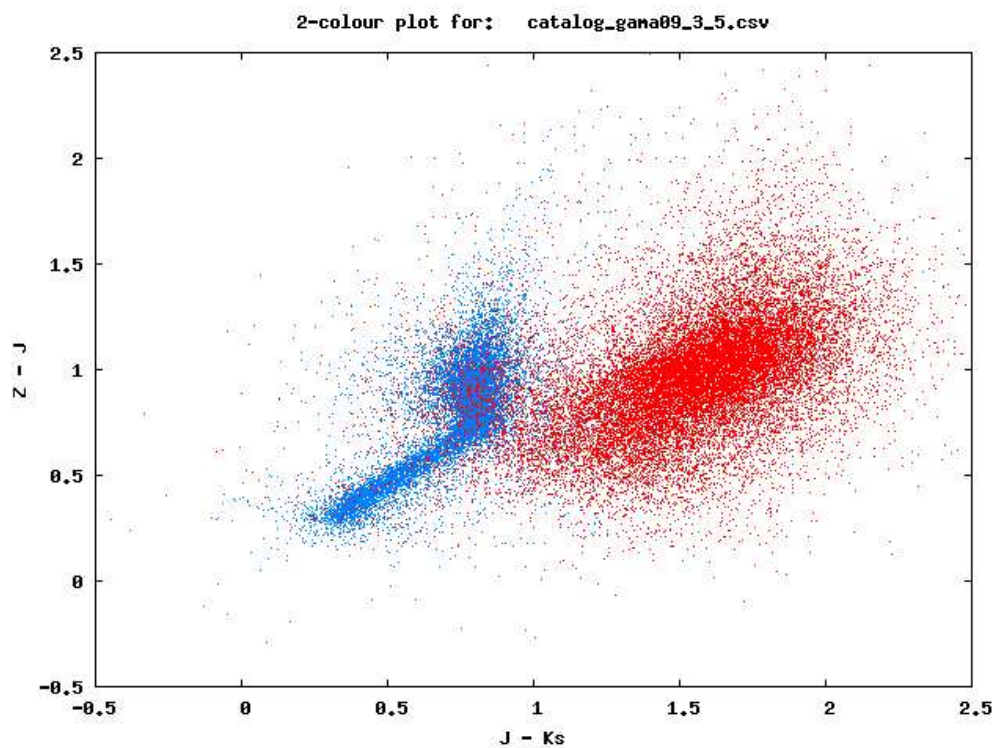


Figure 3: Two-colour diagram,  $Z-J$  vs  $J-K_s$ , for one tile, selecting objects with  $J < 20$ . Stellar objects are blue points, extended objects are red points.

## Appendix 1: summary of all columns in the band-merged VIKING catalogue

| Column Name     | Type     | Length<br>(byte) | Unit    | Description   | Default Value   | Unified Content<br>Descriptor |
|-----------------|----------|------------------|---------|---|---|-------------------------------|
| sourceID        | bigint   | 8                |         | UID (unique over entire VSA via programme ID prefix)<br>of this merged detection as assigned by merge algorithm |   | ID_MAIN                       |
| cuEventID       | int      | 4                |         | UID of curation event giving rise to this record  |   | REFER_CODE                    |
| frameSetID      | bigint   | 8                |         | UID of the set of frames that this merged source comes from   |   | REFER_CODE                    |
| ra              | float    | 8                | Degrees | Celestial Right Ascension   |   | POS_EQ_RA_MAIN                |
| dec             | float    | 8                | Degrees | Celestial Declination   |   | POS_EQ_DEC_MAIN               |
| cx              | float    | 8                |         | unit vector of spherical co-ordinates   |   | POS_EQ_X                      |
| cy              | float    | 8                |         | unit vector of spherical co-ordinates   |   | POS_EQ_Y                      |
| cz              | float    | 8                |         | unit vector of spherical co-ordinates   |   | POS_EQ_Z                      |
| htmID           | bigint   | 8                |         | Hierarchical Triangular Mesh (HTM) index,<br>20 deep, for equatorial co-ordinates                               |   | POS_GENERAL                   |
| l               | float    | 8                | Degrees | Galactic longitude  |   | POS_GAL_LON                   |
| b               | float    | 8                | Degrees | Galactic latitude   |   | POS_GAL_LAT                   |
| lambda          | float    | 8                | Degrees | SDSS system spherical co-ordinate 1   |   | POS                           |
| eta             | float    | 8                | Degrees | SDSS system spherical co-ordinate 2   |   | POS                           |
| priOrSec        | bigint   | 8                |         | Seam code for a unique (=0) or<br>duplicated (!=0) source (eg. flags overlap duplicates).                       | -99999999   | CODE_MISC                     |
| zmyPnt          | real     | 4                | mag     | Point source colour Z-Y (using aperMag3)  | -0.9999995e9  | PHOT_COLOR                    |
| zmyPntErr       | real     | 4                | mag     | Error on point source colour Z-Y  | -0.9999995e9  | ERROR                         |
| ymjPnt          | real     | 4                | mag     | Point source colour Y-J (using aperMag3)  | -0.9999995e9  | PHOT_COLOR                    |
| ymjPntErr       | real     | 4                | mag     | Error on point source colour Y-J  | -0.9999995e9  | ERROR                         |
| jmhPnt          | real     | 4                | mag     | Point source colour J-H (using aperMag3)  | -0.9999995e9  | PHOT_COLOR                    |
| jmhPntErr       | real     | 4                | mag     | Error on point source colour J-H  | -0.9999995e9  | ERROR                         |
| hmksPnt         | real     | 4                | mag     | Point source colour H-K <sub>s</sub> (using aperMag3)   | -0.9999995e9  | PHOT_COLOR                    |
| hmksPntErr      | real     | 4                | mag     | Error on point source colour H-K <sub>s</sub>   | -0.9999995e9  | ERROR                         |
| zmyExt          | real     | 4                | mag     | Extended source colour Z-Y (using aperMagNoAperCorr3)   | -0.9999995e9  | PHOT_COLOR                    |
| zmyExtErr       | real     | 4                | mag     | Error on extended source colour Z-Y   | -0.9999995e9  | ERROR                         |
| ymjExt          | real     | 4                | mag     | Extended source colour Y-J (using aperMagNoAperCorr3)   | -0.9999995e9  | PHOT_COLOR                    |
| ymjExtErr       | real     | 4                | mag     | Error on extended source colour Y-J   | -0.9999995e9  | ERROR                         |
| jmhExt          | real     | 4                | mag     | Extended source colour J-H (using aperMagNoAperCorr3)   | -0.9999995e9  | PHOT_COLOR                    |
| jmhExtErr       | real     | 4                | mag     | Error on extended source colour J-H   | -0.9999995e9  | ERROR                         |
| hmksExt         | real     | 4                | mag     | Extended source colour H-K <sub>s</sub> (using aperMagNoAperCorr3)  | -0.9999995e9  | PHOT_COLOR                    |
| hmksExtErr      | real     | 4                | mag     | Error on extended source colour H-K <sub>s</sub>  | -0.9999995e9  | ERROR                         |
| mergedClassStat | real     | 4                |         | Merged N(0,1) stellarness-of-profile statistic  | -0.9999995e9  | STAT_PROP                     |
| mergedClass     | smallint | 2                |         | Class flag from available measurements  | 1=galaxy<br>0=noise<br>-1=stellar<br>-2=probableStar<br>-3=probableGalaxy<br>-9=saturated | CODE_MISC                     |

|                     |      |   |     |   |              |           |
|---------------------|------|---|-----|---|--------------|-----------|
| pStar               | real | 4 |     | Probability that the source is a star   |              | STAT_PROP |
| pGalaxy             | real | 4 |     | Probability that the source is a galaxy   |              | STAT_PROP |
| pNoise              | real | 4 |     | Probability that the source is noise  |              | STAT_PROP |
| pSaturated          | real | 4 |     | Probability that the source is saturated  |              | STAT_PROP |
| eBV                 | real | 4 |     | The galactic dust extinction value measured from the Schlegel, Finkbeiner & Davis (1998) maps. This uses the correction given in Bonifacio, Monai & Beers (2000). This correction reduces the extinction value in regions of high extinction ( $E(B-V) > 0.1$ ) | -0.9999995e9 |           |
| aZ                  | real | 4 | mag | The galactic extinction correction in the Z band for extragalactic objects  | -0.9999995e9 |           |
| aY                  | real | 4 | mag | The galactic extinction correction in the Y band for extragalactic objects  | -0.9999995e9 |           |
| aJ                  | real | 4 | mag | The galactic extinction correction in the J band for extragalactic objects  | -0.9999995e9 |           |
| aH                  | real | 4 | mag | The galactic extinction correction in the H band for extragalactic objects  | -0.9999995e9 |           |
| aKs                 | real | 4 | mag | The galactic extinction correction in the K <sub>s</sub> band for extragalactic objects   | -0.9999995e9 |           |
| zPetroMag           | real | 4 | mag | Extended source Z mag (Petrosian)   | -0.9999995e9 | PHOT_MAG  |
| zPetroMagErr        | real | 4 | mag | Error in extended source Z mag (Petrosian)  | -0.9999995e9 | ERROR     |
| zPsfMag             | real | 4 | mag | Point source profile-fitted Z mag   | -0.9999995e9 | PHOT_MAG  |
| zPsfMagErr          | real | 4 | mag | Error in point source profile-fitted Z mag  | -0.9999995e9 | ERROR     |
| zSerMag2D           | real | 4 | mag | Extended source Z mag (profile-fitted)  | -0.9999995e9 | PHOT_MAG  |
| zSerMag2DErr        | real | 4 | mag | Error in extended source Z mag (profile-fitted)   | -0.9999995e9 | ERROR     |
| zAperMag3           | real | 4 | mag | Default point source Z aperture corrected mag (2.0 arcsec aperture diameter)  | -0.9999995e9 | PHOT_MAG  |
| zAperMag3Err        | real | 4 | mag | Error in default point/extended source Z mag (2.0 arcsec aperture diameter)   | -0.9999995e9 | ERROR     |
| zAperMag4           | real | 4 | mag | Point source Z aperture corrected mag (2.8 arcsec aperture diameter)  | -0.9999995e9 | PHOT_MAG  |
| zAperMag4Err        | real | 4 | mag | Error in point/extended source Z mag (2.8 arcsec aperture diameter)   | -0.9999995e9 | ERROR     |
| zAperMag6           | real | 4 | mag | Point source Z aperture corrected mag (5.7 arcsec aperture diameter)  | -0.9999995e9 | PHOT_MAG  |
| zAperMag6Err        | real | 4 | mag | Error in point/extended source Z mag (5.7 arcsec aperture diameter)   | -0.9999995e9 | ERROR     |
| zAperMagNoAperCorr3 | real | 4 | mag | Default extended source Z aperture mag (2.0 arcsec aperture diameter)   | -0.9999995e9 | PHOT_MAG  |
| zAperMagNoAperCorr4 | real | 4 | mag | Extended source Z aperture mag (2.8 arcsec aperture diameter)   | -0.9999995e9 | PHOT_MAG  |
| zAperMagNoAperCorr6 | real | 4 | mag | Extended source Z aperture mag (5.7 arcsec aperture diameter)   | -0.9999995e9 | PHOT_MAG  |

|                     |          |   |         |   |              |                  |
|---------------------|----------|---|---------|---|--------------|------------------|
| zHICorSMjRadAs      | real     | 4 | arcsec  | Seeing corrected half-light, semi-major axis in Z band                          | -0.9999995e9 | EXTENSION_RAD    |
| zGausig             | real     | 4 | pixels  | RMS of axes of ellipse fit in Z   | -0.9999995e9 | MORPH_PARAM      |
| zEll                | real     | 4 |         | 1-b/a, where a/b=semi-major/minor axes in Z                                     | -0.9999995e9 | PHYS_ELLIPTICITY |
| zPA                 | real     | 4 | Degrees | ellipse fit celestial orientation in Z  | -0.9999995e9 | POS_POS-ANG      |
| zErrBits            | int      | 4 |         | processing warning/error bitwise flags in Z                                     | -99999999    | CODE_MISC        |
| zAverageConf        | real     | 4 |         | average confidence in 2 arcsec diameter default aperture Z                      | -99999999    | CODE_MISC        |
| zClass              | smallint | 2 |         | discrete image classification flag in Z   | -9999        | CLASS_MISC       |
| zClassStat          | real     | 4 |         | N(0,1) stellarness-of-profile statistic in Z                                    | -0.9999995e9 | STAT_PROP        |
| zppErrBits          | int      | 4 |         | additional WFAU post-processing error bits in Z                                 | 0            | CODE_MISC        |
| zSeqNum             | int      | 4 |         | the running number of the Z detection -99999999                                 |              | ID_NUMBER        |
| zXi                 | real     | 4 | arcsec  | Offset of Z detection from master position (+east/-west)                        | -0.9999995e9 | POS_EQ_RA_OFF    |
| zEta                | real     | 4 | arcsec  | Offset of Z detection from master position (+north/-south)                      | -0.9999995e9 | POS_EQ_DEC_OFF   |
| yPetroMag           | real     | 4 | mag     | Extended source Y mag (Petrosian)   | -0.9999995e9 | PHOT_MAG         |
| yPetroMagErr        | real     | 4 | mag     | Error in extended source Y mag (Petrosian)                                      | -0.9999995e9 | ERROR            |
| yPsfMag             | real     | 4 | mag     | Point source profile-fitted Y mag   | -0.9999995e9 | PHOT_MAG         |
| yPsfMagErr          | real     | 4 | mag     | Error in point source profile-fitted Y mag                                      | -0.9999995e9 | ERROR            |
| ySerMag2D           | real     | 4 | mag     | Extended source Y mag (profile-fitted)  | -0.9999995e9 | PHOT_MAG         |
| ySerMag2DErr        | real     | 4 | mag     | Error in extended source Y mag (profile-fitted)                                 | -0.9999995e9 | ERROR            |
| yAperMag3           | real     | 4 | mag     | Default point source Y aperture corrected mag<br>(2.0 arcsec aperture diameter) | -0.9999995e9 | PHOT_MAG         |
| yAperMag3Err        | real     | 4 | mag     | Error in default point/extended source Y mag<br>(2.0 arcsec aperture diameter)  | -0.9999995e9 | ERROR            |
| yAperMag4           | real     | 4 | mag     | Point source Y aperture corrected mag<br>(2.8 arcsec aperture diameter)         | -0.9999995e9 | PHOT_MAG         |
| yAperMag4Err        | real     | 4 | mag     | Error in point/extended source Y mag<br>(2.8 arcsec aperture diameter)          | -0.9999995e9 | ERROR            |
| yAperMag6           | real     | 4 | mag     | Point source Y aperture corrected mag<br>(5.7 arcsec aperture diameter)         | -0.9999995e9 | PHOT_MAG         |
| yAperMag6Err        | real     | 4 | mag     | Error in point/extended source Y mag<br>(5.7 arcsec aperture diameter)          | -0.9999995e9 | ERROR            |
| yAperMagNoAperCorr3 | real     | 4 | mag     | Default extended source Y aperture mag<br>(2.0 arcsec aperture diameter)        | -0.9999995e9 | PHOT_MAG         |
| yAperMagNoAperCorr4 | real     | 4 | mag     | Extended source Y aperture mag<br>(2.8 arcsec aperture diameter)                | -0.9999995e9 | PHOT_MAG         |
| yAperMagNoAperCorr6 | real     | 4 | mag     | Extended source Y aperture mag<br>(5.7 arcsec aperture diameter)                | -0.9999995e9 | PHOT_MAG         |
| yHICorSMjRadAs      | real     | 4 | arcsec  | Seeing corrected half-light, semi-major axis in Y band                          | -0.9999995e9 | EXTENSION_RAD    |
| yGausig             | real     | 4 | pixels  | RMS of axes of ellipse fit in Y   | -0.9999995e9 | MORPH_PARAM      |
| yEll                | real     | 4 |         | 1-b/a, where a/b=semi-major/minor axes in Y                                     | -0.9999995e9 | PHYS_ELLIPTICITY |
| yPA                 | real     | 4 | Degrees | ellipse fit celestial orientation in Y  | -0.9999995e9 | POS_POS-ANG      |
| yErrBits            | int      | 4 |         | processing warning/error bitwise flags in Y                                     | -99999999    | CODE_MISC        |
| yAverageConf        | real     | 4 |         | average confidence in 2 arcsec diameter default aperture Y                      | -99999999    | CODE_MISC        |
| yClass              | smallint | 2 |         | discrete image classification flag in Y   | -9999        | CLASS_MISC       |
| yClassStat          | real     | 4 |         | N(0,1) stellarness-of-profile statistic in Y                                    | -0.9999995e9 | STAT_PROP        |
| yppErrBits          | int      | 4 |         | additional WFAU post-processing error bits in Y                                 | 0            | CODE_MISC        |

|                     |          |   |         |   |              |                  |
|---------------------|----------|---|---------|---|--------------|------------------|
| ySeqNum             | int      | 4 |         | the running number of the Y detection   | -99999999    | ID_NUMBER        |
| yXi                 | real     | 4 | arcsec  | Offset of Y detection from master position (+east/-west)                        | -0.9999995e9 | POS_EQ_RA_OFF    |
| yEta                | real     | 4 | arcsec  | Offset of Y detection from master position (+north/-south)                      | -0.9999995e9 | POS_EQ_DEC_OFF   |
| jPetroMag           | real     | 4 | mag     | Extended source J mag (Petrosian)   | -0.9999995e9 | PHOT_MAG         |
| jPetroMagErr        | real     | 4 | mag     | Error in extended source J mag (Petrosian)                                      | -0.9999995e9 | ERROR            |
| jPsfMag             | real     | 4 | mag     | Point source profile-fitted J mag   | -0.9999995e9 | PHOT_MAG         |
| jPsfMagErr          | real     | 4 | mag     | Error in point source profile-fitted J mag                                      | -0.9999995e9 | ERROR            |
| jSerMag2D           | real     | 4 | mag     | Extended source J mag (profile-fitted)  | -0.9999995e9 | PHOT_MAG         |
| jSerMag2DErr        | real     | 4 | mag     | Error in extended source J mag (profile-fitted)                                 | -0.9999995e9 | ERROR            |
| jAperMag3           | real     | 4 | mag     | Default point source J aperture corrected mag<br>(2.0 arcsec aperture diameter) | -0.9999995e9 | PHOT_MAG         |
| jAperMag3Err        | real     | 4 | mag     | Error in default point/extended source J mag<br>(2.0 arcsec aperture diameter)  | -0.9999995e9 | ERROR            |
| jAperMag4           | real     | 4 | mag     | Point source J aperture corrected mag<br>(2.8 arcsec aperture diameter)         | -0.9999995e9 | PHOT_MAG         |
| jAperMag4Err        | real     | 4 | mag     | Error in point/extended source J mag<br>(2.8 arcsec aperture diameter)          | -0.9999995e9 | ERROR            |
| jAperMag6           | real     | 4 | mag     | Point source J aperture corrected mag<br>(5.7 arcsec aperture diameter)         | -0.9999995e9 | PHOT_MAG         |
| jAperMag6Err        | real     | 4 | mag     | Error in point/extended source J mag<br>(5.7 arcsec aperture diameter)          | -0.9999995e9 | ERROR            |
| jAperMagNoAperCorr3 | real     | 4 | mag     | Default extended source J aperture mag<br>(2.0 arcsec aperture diameter)        | -0.9999995e9 | PHOT_MAG         |
| jAperMagNoAperCorr4 | real     | 4 | mag     | Extended source J aperture mag<br>(2.8 arcsec aperture diameter)                | -0.9999995e9 | PHOT_MAG         |
| jAperMagNoAperCorr6 | real     | 4 | mag     | Extended source J aperture mag<br>(5.7 arcsec aperture diameter)                | -0.9999995e9 | PHOT_MAG         |
| jHlCorSMjRadAs      | real     | 4 | arcsec  | Seeing corrected half-light, semi-major axis in J band                          | -0.9999995e9 | EXTENSION_RAD    |
| jGausig             | real     | 4 | pixels  | RMS of axes of ellipse fit in J   | -0.9999995e9 | MORPH_PARAM      |
| jEll                | real     | 4 |         | 1-b/a, where a/b=semi-major/minor axes in J                                     | -0.9999995e9 | PHYS_ELLIPTICITY |
| jPA                 | real     | 4 | Degrees | ellipse fit celestial orientation in J  | -0.9999995e9 | POS_POS-ANG      |
| jErrBits            | int      | 4 |         | processing warning/error bitwise flags in J                                     | -99999999    | CODE_MISC        |
| jAverageConf        | real     | 4 |         | average confidence in 2 arcsec diameter default aperture J                      | -99999999    | CODE_MISC        |
| jClass              | smallint | 2 |         | discrete image classification flag in J   | -9999        | CLASS_MISC       |
| jClassStat          | real     | 4 |         | N(0,1) stellarness-of-profile statistic in J                                    | -0.9999995e9 | STAT_PROP        |
| jppErrBits          | int      | 4 |         | additional WFAU post-processing error bits in J                                 | 0            | CODE_MISC        |
| jSeqNum             | int      | 4 |         | the running number of the J detection   | -99999999    | ID_NUMBER        |
| jXi                 | real     | 4 | arcsec  | Offset of J detection from master position (+east/-west)                        | -0.9999995e9 | POS_EQ_RA_OFF    |
| jEta                | real     | 4 | arcsec  | Offset of J detection from master position (+north/-south)                      | -0.9999995e9 | POS_EQ_DEC_OFF   |

|                     |      |        |         |   |              |                  |
|---------------------|------|--------|---------|---|--------------|------------------|
| hPetroMag           | real | 4      | mag     | Extended source H mag (Petrosian)   | -0.9999995e9 | PHOT_MAG         |
| hPetroMagErr        | real | 4      | mag     | Error in extended source H mag (Petrosian)                                      | -0.9999995e9 | ERROR            |
| hPsfMag             | real | 4      | mag     | Point source profile-fitted H mag   | -0.9999995e9 | PHOT_MAG         |
| hPsfMagErr          | real | 4      | mag     | Error in point source profile-fitted H mag                                      | -0.9999995e9 | ERROR            |
| hSerMag2D           | real | 4      | mag     | Extended source H mag (profile-fitted)  | -0.9999995e9 | PHOT_MAG         |
| hSerMag2DErr        | real | 4      | mag     | Error in extended source H mag (profile-fitted)                                 | -0.9999995e9 | ERROR            |
| hAperMag3           | real | 4      | mag     | Default point source H aperture corrected mag<br>(2.0 arcsec aperture diameter) | -0.9999995e9 | PHOT_MAG         |
| hAperMag3Err        | real | 4      | mag     | Error in default point/extended source H mag<br>(2.0 arcsec aperture diameter)  | -0.9999995e9 | ERROR            |
| hAperMag4           | real | 4      | mag     | Point source H aperture corrected mag<br>(2.8 arcsec aperture diameter)         | -0.9999995e9 | PHOT_MAG         |
| hAperMag4Err        | real | 4      | mag     | Error in point/extended source H mag<br>(2.8 arcsec aperture diameter)          | -0.9999995e9 | ERROR            |
| hAperMag6           | real | 4      | mag     | Point source H aperture corrected mag<br>(5.7 arcsec aperture diameter)         | -0.9999995e9 | PHOT_MAG         |
| hAperMag6Err        | real | 4      | mag     | Error in point/extended source H mag<br>(5.7 arcsec aperture diameter)          | -0.9999995e9 | ERROR            |
| hAperMagNoAperCorr3 | real | 4      | mag     | Default extended source H aperture mag<br>(2.0 arcsec aperture diameter)        | -0.9999995e9 | PHOT_MAG         |
| hAperMagNoAperCorr4 | real | 4      | mag     | Extended source H aperture mag<br>(2.8 arcsec aperture diameter)                | -0.9999995e9 | PHOT_MAG         |
| hAperMagNoAperCorr6 | real | 4      | mag     | Extended source H aperture mag<br>(5.7 arcsec aperture diameter)                | -0.9999995e9 | PHOT_MAG         |
| hHICorSMjRadAs      | real | 4      | arcsec  | Seeing corrected half-light, semi-major axis in H band                          | -0.9999995e9 | EXTENSION_RAD    |
| hGausig             | real | 4      | pixels  | RMS of axes of ellipse fit in H   | -0.9999995e9 | MORPH_PARAM      |
| hEll                | real | 4      |         | 1-b/a, where a/b=semi-major/minor axes in H                                     | -0.9999995e9 | PHYS_ELLIPTICITY |
| hPA                 | real | 4      | Degrees | ellipse fit celestial orientation in H  | -0.9999995e9 | POS_POS-ANG      |
| hErrBits            | int  | 4      |         | processing warning/error bitwise flags in H                                     | -99999999    | CODE_MISC        |
| hAverageConf        | real | 4      |         | average confidence in 2 arcsec diameter default aperture H                      | -99999999    | CODE_MISC        |
| hClass              | smal | lint 2 |         | discrete image classification flag in H   | -9999        | CLASS_MISC       |
| hClassStat          | real | 4      |         | N(0,1) stellarness-of-profile statistic in H                                    | -0.9999995e9 | STAT_PROP        |
| hppErrBits          | int  | 4      |         | additional WFAU post-processing error bits in H                                 | 0            | CODE_MISC        |
| hSeqNum             | int  | 4      |         | the running number of the H detection   | -99999999    | ID_NUMBER        |
| hXi                 | real | 4      | arcsec  | Offset of H detection from master position (+east/-west)                        | -0.9999995e9 | POS_EQ_RA_OFF    |
| hEta                | real | 4      | arcsec  | Offset of H detection from master position (+north/-south)                      | -0.9999995e9 | POS_EQ_DEC_OFF   |



|                      |          |   |         |   |              |                  |
|----------------------|----------|---|---------|---|--------------|------------------|
| ksPetroMag           | real     | 4 | mag     | Extended source $K_s$ mag (Petrosian)   | -0.9999995e9 | PHOT_MAG         |
| ksPetroMagErr        | real     | 4 | mag     | Error in extended source $K_s$ mag (Petrosian)                                      | -0.9999995e9 | ERROR            |
| ksPsfMag             | real     | 4 | mag     | Point source profile-fitted $K_s$ mag   | -0.9999995e9 | PHOT_MAG         |
| ksPsfMagErr          | real     | 4 | mag     | Error in point source profile-fitted $K_s$ mag                                      | -0.9999995e9 | ERROR            |
| ksSerMag2D           | real     | 4 | mag     | Extended source $K_s$ mag (profile-fitted)  | -0.9999995e9 | PHOT_MAG         |
| ksSerMag2DErr        | real     | 4 | mag     | Error in extended source $K_s$ mag (profile-fitted)                                 | -0.9999995e9 | ERROR            |
| ksAperMag3           | real     | 4 | mag     | Default point source $K_s$ aperture corrected mag<br>(2.0 arcsec aperture diameter) | -0.9999995e9 | PHOT_MAG         |
| ksAperMag3Err        | real     | 4 | mag     | Error in default point/extended source $K_s$ mag<br>(2.0 arcsec aperture diameter)  | -0.9999995e9 | ERROR            |
| ksAperMag4           | real     | 4 | mag     | Point source $K_s$ aperture corrected mag<br>(2.8 arcsec aperture diameter)         | -0.9999995e9 | PHOT_MAG         |
| ksAperMag4Err        | real     | 4 | mag     | Error in point/extended source $K_s$ mag<br>(2.8 arcsec aperture diameter)          | -0.9999995e9 | ERROR            |
| ksAperMag6           | real     | 4 | mag     | Point source $K_s$ aperture corrected mag<br>(5.7 arcsec aperture diameter)         | -0.9999995e9 | PHOT_MAG         |
| ksAperMag6Err        | real     | 4 | mag     | Error in point/extended source $K_s$ mag<br>(5.7 arcsec aperture diameter)          | -0.9999995e9 | ERROR            |
| ksAperMagNoAperCorr3 | real     | 4 | mag     | Default extended source $K_s$ aperture mag<br>(2.0 arcsec aperture diameter)        | -0.9999995e9 | PHOT_MAG         |
| ksAperMagNoAperCorr4 | real     | 4 | mag     | Extended source $K_s$ aperture mag<br>(2.8 arcsec aperture diameter)                | -0.9999995e9 | PHOT_MAG         |
| ksAperMagNoAperCorr6 | real     | 4 | mag     | Extended source $K_s$ aperture mag<br>(5.7 arcsec aperture diameter)                | -0.9999995e9 | PHOT_MAG         |
| ksHlCorSMjRadAs      | real     | 4 | arcsec  | Seeing corrected half-light, semi-major axis in $K_s$ band                          | -0.9999995e9 | EXTENSION_RAD    |
| ksGausig             | real     | 4 | pixels  | RMS of axes of ellipse fit in $K_s$   | -0.9999995e9 | MORPH_PARAM      |
| ksEll                | real     | 4 |         | 1-b/a, where a/b=semi-major/minor axes in $K_s$                                     | -0.9999995e9 | PHYS_ELLIPTICITY |
| ksPA                 | real     | 4 | Degrees | ellipse fit celestial orientation in $K_s$  | -0.9999995e9 | POS_POS-ANG      |
| ksErrBits            | int      | 4 |         | processing warning/error bitwise flags in $K_s$                                     | -99999999    | CODE_MISC        |
| ksAverageConf        | real     | 4 |         | average confidence in 2 arcsec diameter default aperture $K_s$                      | -99999999    | CODE_MISC        |
| ksClass              | smallint | 2 |         | discrete image classification flag in $K_s$   | -9999        | CLASS_MISC       |
| ksClassStat          | real     | 4 |         | N(0,1) stellarness-of-profile statistic in $K_s$                                    | -0.9999995e9 | STAT_PROP        |
| ksppErrBits          | int      | 4 |         | additional WFAU post-processing error bits in $K_s$                                 | 0            | CODE_MISC        |
| ksSeqNum             | int      | 4 |         | the running number of the $K_s$ detection   | -99999999    | ID_NUMBER        |
| ksXi                 | real     | 4 | arcsec  | Offset of $K_s$ detection from master position (+east/-west)                        | -0.9999995e9 | POS_EQ_RA_OFF    |
| ksEta                | real     | 4 | arcsec  | Offset of $K_s$ detection from master position (+north/-south)                      | -0.9999995e9 | POS_EQ_DEC_OFF   |
| primary_source       | smallint | 2 |         | to select between multiple entries in the catalogue                                 | 0            | PRIMARY_SOURCE   |